Journal of Solid Mechanics Vol. 6, No. 2 (2014) pp. 158-172

Stress Analysis of Skew Nanocomposite Plates Based on 3D Elasticity Theory Using Differential Quadrature Method

M.R. Nami, M. Janghorban*

School of Mechanical Engineering, Shiraz University, Shiraz, Iran

Received 21 February 2014; accepted 11 April 2014

ABSTRACT

In this paper, a three dimensional analysis of arbitrary straight-sided quadrilateral nanocomposite plates are investigated. The governing equations are based on three-dimensional elasticity theory which can be used for both thin and thick nanocomposite plates. Although the equations can support all the arbitrary straight-sided quadrilateral plates but as a special case, the numerical results for skew nanocomposite plates are investigated. The differential quadrature method (DQM) is used to solve these equations. In order to show the accuracy of present work, our results are compared with other numerical solution for skew plates. From the knowledge of author, it is the first time that the stress analysis of arbitrary straight-sided quadrilateral nanocomposite plates is investigated. It is shown that increasing the skew angle and thickness of nanocomposite skew plate will decrease the vertical displacements. It is also noted that the thermal effects are also added in the governing equations.

Keywords: Straight-sided quadrilateral nanocomposite plates; 3D elasticity theory; Differential quadrature method; Thermal environment

1 INTRODUCTION

THE discovery of carbon nanotubes has initiated a number of scientific investigations to explore their unique properties and potential applications. The composite community considers carbon nanotubes as ideal reinforcements for structural and multifunctional composite applications [1]. Shariyat, and Darabi [2] studied the characteristics of low/medium velocity impact responses of thin nanocomposite plates impacted by rigid spherical indenters. A modified contact law that takes into account effects of the plate thickness and boundary conditions was employed in this research. Jafari Mehrabadi et al [3] investigated the mechanical buckling of a functionally graded nanocomposite rectangular plate reinforced by aligned and straight single-walled carbon nanotubes subjected to uniaxial and biaxial in-plane loadings. Belay and Kiselev [4] presented the results of molecular dynamics simulation of deformation and fracture of a "copper - molybdenum" nanocomposite plate under uniaxial tension. It was shown that plastic deformation in shear bands in the copper culminates in the pore formation at the Cu-Mo contact boundary. Yas et al [5] studied the vibrational properties of functionally graded nanocomposite cylindrical panels reinforced by single-walled carbon nanotubes based on the three-dimensional theory of elasticity. The carbon nanotube reinforced cylindrical panel had smooth variation of carbon nanotube fraction in the radial direction and the material properties were estimated by the extended rule of mixture. Dynamic analysis of nanocomposite cylinders reinforced by single-walled carbon nanotubes subjected to an impact load was carried out by a mesh-free method by Moradi-Dastjerdi et al [6]. Free vibration and stress wave propagation analysis of carbon nanotube

* Corresponding author.
E-mail address: maziar.janghorban@gmail.com (M. Janghorban).

reinforced composite cylinders were presented. Heshmati and Yas [7] studied the dynamic response of functionally graded multi-walled carbon nanotube polystyrene nanocomposite beams subjected to multi-moving loads based on Timoshenko beam theory. The finite element method was employed to discretize the model and obtain a numerical approximation of the motion equation. Postbuckling analysis was presented for nanocomposite cylindrical shells reinforced by single-walled carbon nanotubes subjected to combined axial and radial mechanical loads in thermal environment by Shen and Xiang [8]. The governing equations were based on a higher order shear deformation shell theory with a von Kármán-type of kinematic nonlinearity.

Skew and trapezoidal plates have quite a good number of applications in modern structures. Skew plate structures can be found frequently in modern construction in the form of reinforced slabs or stiffened plates. Such structures are widely used as floors in bridges, ship hulls, buildings, etc. Several researchers have addressed the linear and nonlinear static and dynamic problems of skew and trapezoidal plates [9-18].

In this research, based on three-dimensional elasticity theory, the equations for the arbitrary straight-sided quadrilateral nanocomposite plates are achieved. In the derivation of these equations, the thermal effect is included so other researchers can extend present work for thermal environment, too. The equations are solved with differential quadrature method. As a special case of straight-sided quadrilateral plates, the displacements and stresses are calculated for skew nanocomposite plates. The author hopes that the present work can be a new step in investigation of nanocomposites.

2 MATERIAL PROPERTIES

In this work, the numerical results of molecular dynamics simulation for the analysis of nanocomposites (Fig. 1) by Griebal and Hamaekers [19,25] are used. All their tensile test simulations were carried out under normal condition. The same time steps and fictitious masses as in the molecular dynamics part of the equilibration process were used [19]. To apply a tensile load to one of the six independent stress components, they used a stress rate of $0.01 Gpa/ps$. A molecular dynamics tensile simulation was stopped when a strain of 10% was reached [19]. Some of the elastic constant for nanocomposites can be found as [19,25],

$$C_{11} = 2.3684 Gpa, C_{12} = 0.9232 Gpa, C_{13} = 0.8511 Gpa, C_{22} = 2.4118 Gpa, C_{23} = 0.8852 Gpa, C_{33} = 23.7746 Gpa,$$
$$C_{44} = 0.9578 Gpa, C_{55} = 0.8980 Gpa, C_{66} = 0.67897 Gpa$$

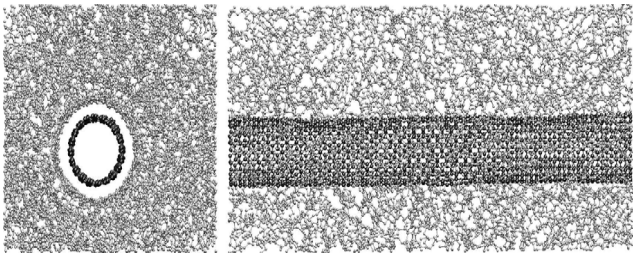

Fig. 1
Left: Front view of unit cell. Right: Side view of the unit cell [19].

3 GOVERNING EQUATIONS

In the following equations, the general stress-strain relation with linear behavior is presented. The stress-strain relations in general form can be written as follow [24],

$$\begin{aligned}
\sigma_{11} &= C_{11}\varepsilon_{11} + C_{12}\varepsilon_{22} + C_{13}\varepsilon_{33} + C_{14}\gamma_{23} + C_{15}\gamma_{13} + C_{16}\gamma_{12} \\
\sigma_{22} &= C_{21}\varepsilon_{11} + C_{22}\varepsilon_{22} + C_{23}\varepsilon_{33} + C_{24}\gamma_{23} + C_{25}\gamma_{13} + C_{26}\gamma_{12} \\
\sigma_{33} &= C_{31}\varepsilon_{11} + C_{32}\varepsilon_{22} + C_{33}\varepsilon_{33} + C_{34}\gamma_{23} + C_{35}\gamma_{13} + C_{46}\gamma_{12} \\
\tau_{23} &= C_{41}\varepsilon_{11} + C_{42}\varepsilon_{22} + C_{43}\varepsilon_{33} + C_{44}\gamma_{23} + C_{45}\gamma_{13} + C_{46}\gamma_{12} \\
\tau_{13} &= C_{51}\varepsilon_{11} + C_{52}\varepsilon_{22} + C_{53}\varepsilon_{33} + C_{54}\gamma_{23} + C_{55}\gamma_{13} + C_{56}\gamma_{12} \\
\tau_{12} &= C_{61}\varepsilon_{11} + C_{62}\varepsilon_{22} + C_{63}\varepsilon_{33} + C_{64}\gamma_{23} + C_{65}\gamma_{13} + C_{66}\gamma_{12}
\end{aligned} \tag{1}$$

The equilibrium equations for investigating nanocomposite plates are [24],

$$\begin{aligned}
\partial\sigma_x/\partial x + \partial\tau_{xy}/\partial y + \partial\tau_{zx}/\partial z &= \rho\partial^2 u/\partial t^2 \\
\partial\sigma_y/\partial y + \partial\tau_{xy}/\partial x + \partial\tau_{zy}/\partial z &= \rho\partial^2 v/\partial t^2 \\
\partial\sigma_z/\partial z + \partial\tau_{yz}/\partial y + \partial\tau_{xz}/\partial x &= \rho\partial^2 w/\partial t^2
\end{aligned} \tag{2}$$

where $\sigma_{ij}\,(i,j=x,y,z)$ are the stress tensor components; ε_{ii} and $\gamma_{ij}\,(i,j=x,y,z;i\neq j)$ are the normal and shearing components of the strain tensor, respectively. The linear strain-displacements relations can be written as follow [24],

$$\begin{aligned}
&\varepsilon_x = (\partial u/\partial x) \quad , \quad \varepsilon_y = (\partial v/\partial y) \quad , \quad \varepsilon_z = (\partial w/\partial z) \\
&\gamma_{xy} = (\partial u/\partial y + \partial v/\partial x) \quad , \quad \gamma_{xz} = (\partial u/\partial z + \partial w/\partial x) \quad , \quad \gamma_{yz} = (\partial v/\partial z + \partial w/\partial y)
\end{aligned} \tag{3}$$

where *u,v* and *w* are the displacements in the *x,y* and *z* directions. Now by substituting Eq. (3) in Eqs. (1-2), the general governing equations for triclinic rectangular plates are,

$$\begin{aligned}
&\partial\{C_{11}\partial u/\partial x + C_{12}\partial v/\partial y + C_{13}\partial w/\partial z + C_{14}(\partial v/\partial z + \partial w/\partial y) + C_{15}(\partial u/\partial z + \partial w/\partial x) + C_{16}(\partial u/\partial y + \partial v/\partial x)\}/\partial x \\
&+\partial\{C_{61}\partial u/\partial x + C_{62}\partial v/\partial y + C_{63}\partial w/\partial z + C_{64}(\partial v/\partial z + \partial w/\partial y) + C_{65}(\partial u/\partial z + \partial w/\partial x) + C_{66}(\partial u/\partial y + \partial v/\partial x)\}/\partial y \\
&+\partial\{C_{51}\partial u/\partial x + C_{52}\partial v/\partial y + C_{53}\partial w/\partial z + C_{54}(\partial v/\partial z + \partial w/\partial y) + C_{55}(\partial u/\partial z + \partial w/\partial x) + C_{56}(\partial u/\partial y + \partial v/\partial x)\}/\partial z \\
&= \rho\partial^2 u/\partial t^2
\end{aligned} \tag{4}$$

$$\begin{aligned}
&\partial\{C_{21}\partial u/\partial x + C_{22}\partial v/\partial y + C_{23}\partial w/\partial z + C_{24}(\partial v/\partial z + \partial w/\partial y) + C_{25}(\partial u/\partial z + \partial w/\partial x) + C_{26}(\partial u/\partial y + \partial v/\partial x)\}/\partial y \\
&+\partial\{C_{61}\partial u/\partial x + C_{62}\partial v/\partial y + C_{63}\partial w/\partial z + C_{64}(\partial v/\partial z + \partial w/\partial y) + C_{65}(\partial u/\partial z + \partial w/\partial x) + C_{66}(\partial u/\partial y + \partial v/\partial x)\}/\partial x \\
&+\partial\{C_{41}\partial u/\partial x + C_{42}\partial v/\partial y + C_{43}\partial w/\partial z + C_{44}(\partial v/\partial z + \partial w/\partial y) + C_{45}(\partial u/\partial z + \partial w/\partial x) + C_{46}(\partial u/\partial y + \partial v/\partial x)\}/\partial z \\
&= \rho\partial^2 v/\partial t^2
\end{aligned} \tag{5}$$

$$\begin{aligned}
&\partial\{C_{31}\partial u/\partial x + C_{32}\partial v/\partial y + C_{33}\partial w/\partial z + C_{34}(\partial v/\partial z + \partial w/\partial y) + C_{35}(\partial u/\partial z + \partial w/\partial x) + C_{36}(\partial u/\partial y + \partial v/\partial x)\}/\partial z \\
&+\partial\{C_{41}\partial u/\partial x + C_{42}\partial v/\partial y + C_{43}\partial w/\partial z + C_{44}(\partial v/\partial z + \partial w/\partial y) + C_{45}(\partial u/\partial z + \partial w/\partial x) + C_{46}(\partial u/\partial y + \partial v/\partial x)\}/\partial y \\
&+\partial\{C_{51}\partial u/\partial x + C_{52}\partial v/\partial y + C_{53}\partial w/\partial z + C_{54}(\partial v/\partial z + \partial w/\partial y) + C_{55}(\partial u/\partial z + \partial w/\partial x) + C_{56}(\partial u/\partial y + \partial v/\partial x)\}/\partial x \\
&= \rho\partial^2 w/\partial t^2
\end{aligned} \tag{6}$$

As shown in Fig. 2, a Cartesian coordinate system (*x*, *y*, *z*) is used to label the material point of the plate in the unstressed reference configuration. It is obvious that the above equations cannot support the arbitrary straight-sided quadrilateral nanocomposite plates and they are suitable for rectangular plates. In order to extend the above equations for arbitrary straight-sided quadrilateral plates, first we rearrange the equations and then we derive the main equations.Using the three-dimensional constitutive relations and the strain-displacement relations, the equilibrium equations in terms of displacement components for a linear elastic plate with infinitesimal deformations can be written as:

In-plane equilibrium:

$$\begin{bmatrix} C_{11} & C_{66} & 0 \\ 0 & 0 & C_{12}+C_{66} \end{bmatrix} \begin{Bmatrix} \dfrac{\partial^2 u_0}{\partial x^2} \\ \dfrac{\partial^2 u_0}{\partial y^2} \\ \dfrac{\partial^2 u_0}{\partial x\,\partial y} \end{Bmatrix} + \begin{bmatrix} 0 & 0 & C_{12}+C_{66} \\ C_{66} & C_{22} & 0 \end{bmatrix} \begin{Bmatrix} \dfrac{\partial^2 v_0}{\partial x^2} \\ \dfrac{\partial^2 v_0}{\partial y^2} \\ \dfrac{\partial^2 v_0}{\partial x\,\partial y} \end{Bmatrix} + \begin{Bmatrix} C_{55}' \dfrac{\partial u_0}{\partial z} + C_{55} \dfrac{\partial^2 u_0}{\partial z^2} \\ C_{44}' \dfrac{\partial v_0}{\partial z} + C_{44} \dfrac{\partial^2 v_0}{\partial z^2} \end{Bmatrix} \tag{7a}$$

$$\begin{bmatrix} C_{55}' & 0 \\ 0 & C_{44}' \end{bmatrix} \begin{Bmatrix} \dfrac{\partial w_0}{\partial x} \\ \dfrac{\partial w_0}{\partial y} \end{Bmatrix} + \begin{bmatrix} C_{13}+C_{55} & 0 \\ 0 & C_{23}+C_{44} \end{bmatrix} \begin{Bmatrix} \dfrac{\partial^2 w_0}{\partial x\,\partial z} \\ \dfrac{\partial^2 w_0}{\partial y\,\partial z} \end{Bmatrix} = \begin{Bmatrix} 0 \\ 0 \end{Bmatrix} \tag{7b}$$

Out-plane-of equilibrium:

$$\begin{aligned} &\begin{bmatrix} C_{13}' & 0 \end{bmatrix} \begin{Bmatrix} \dfrac{\partial u_0}{\partial x} \\ \dfrac{\partial u_0}{\partial y} \end{Bmatrix} + \begin{bmatrix} C_{13}+C_{55} & 0 \end{bmatrix} \begin{Bmatrix} \dfrac{\partial^2 u_0}{\partial x\,\partial z} \\ \dfrac{\partial^2 u_0}{\partial y\,\partial z} \end{Bmatrix} + \begin{bmatrix} 0 & C_{23}' \end{bmatrix} \begin{Bmatrix} \dfrac{\partial v_0}{\partial x} \\ \dfrac{\partial v_0}{\partial y} \end{Bmatrix} + \begin{bmatrix} 0 & C_{23}+C_{44} \end{bmatrix} \begin{Bmatrix} \dfrac{\partial^2 v_0}{\partial x\,\partial z} \\ \dfrac{\partial^2 v_0}{\partial y\,\partial z} \end{Bmatrix} \\ &+ \begin{bmatrix} C_{55} & C_{44} & 0 \end{bmatrix} \begin{Bmatrix} \dfrac{\partial^2 w_0}{\partial x^2} \\ \dfrac{\partial^2 w_0}{\partial y^2} \\ \dfrac{\partial^2 w_0}{\partial x\,\partial y} \end{Bmatrix} + C_{33}' \frac{\partial w_0}{\partial z} + C_{33} \frac{\partial^2 w_0}{\partial z^2} = \left(C_{33}' \alpha + C_{33} \alpha' \right) \Delta T + C_{33} \alpha \frac{d\left(\Delta T\right)}{dz} \end{aligned} \tag{8}$$

where $\left(\ \right)' = \dfrac{d\left(\ \right)}{dz}$. And along the boundary Γ,

$$\delta u_{0n} = n_x \delta u_0 + n_y \delta v_0 = 0 \tag{9a}$$

$$\sigma_{0nn} = n_x^2 \sigma_{0xx} + n_y^2 \sigma_{0yy} + 2 n_x n_y \sigma_{0xy} = 0 \tag{9b}$$

$$\delta u_{0s} = -n_y \delta u_0 + n_x \delta v_0 = 0 \tag{10a}$$

$$\sigma_{0ns} = \left(n_x^2 - n_y^2 \right) \sigma_{0xy} + n_x n_y \left(\sigma_{0yy} - \sigma_{0xx} \right) = 0 \tag{10b}$$

$$\delta w_0 = 0 \tag{11a}$$

$$\sigma_{0nz} = n_x \sigma_{0xz} + n_y \sigma_{0yz} = 0 \tag{11b}$$

At z=0, h:

$$\sigma_{0zx} = 0 \tag{12a}$$

$$\sigma_{0zy} = 0 \tag{12b}$$

$$\sigma_{0zz} = 0 \tag{12c}$$

In order to transform the boundary conditions into the computational domain, they are rearranged as, Eq. (9b):

$$\begin{bmatrix} C_{11}n_x^2 + C_{12}n_y^2 & 2C_{66}n_x n_y \end{bmatrix} \begin{Bmatrix} \frac{\partial u_0}{\partial x} \\ \frac{\partial u_0}{\partial y} \end{Bmatrix} + \begin{bmatrix} 2C_{66}n_x n_y & C_{12}n_x^2 + C_{22}n_y^2 \end{bmatrix} \begin{Bmatrix} \frac{\partial v_0}{\partial x} \\ \frac{\partial v_0}{\partial y} \end{Bmatrix}$$
$$+ \left(C_{13}n_x^2 + C_{23}n_y^2\right)\frac{\partial w_0}{\partial z} = \left[\left(C_{11} + C_{12} + C_{13}\right)n_x^2 + \left(C_{12} + C_{22} + C_{23}\right)n_y^2\right]\alpha\Delta T \tag{13}$$

Eq. (10b):

$$\begin{bmatrix} n_x n_y\left(C_{12} - C_{11}\right) & C_{66}\left(n_x^2 - n_y^2\right) \end{bmatrix} \begin{Bmatrix} \frac{\partial u_0}{\partial x} \\ \frac{\partial u_0}{\partial y} \end{Bmatrix} + \begin{bmatrix} C_{66}\left(n_x^2 - n_y^2\right) & n_x n_y\left(C_{22} - C_{12}\right) \end{bmatrix} \begin{Bmatrix} \frac{\partial v_0}{\partial x} \\ \frac{\partial v_0}{\partial y} \end{Bmatrix}$$
$$+ n_x n_y\left(C_{23} - C_{13}\right)\frac{\partial w_0}{\partial z} = n_x n_y\left(C_{11} + C_{13} - C_{22} - C_{23}\right)\alpha\Delta T \tag{14}$$

Eq. (11b):

$$\begin{bmatrix} C_{55}n_x & C_{44}n_y \end{bmatrix} \begin{Bmatrix} \frac{\partial w_0}{\partial x} \\ \frac{\partial w_0}{\partial y} \end{Bmatrix} + C_{55}n_x\frac{\partial u_0}{\partial z} + C_{44}n_y\frac{\partial v_0}{\partial z} = 0 \tag{15}$$

Eqs. (12a) and (12 b):

$$\begin{Bmatrix} C_{55}\frac{\partial u_0}{\partial z} \\ C_{44}\frac{\partial v_0}{\partial z} \end{Bmatrix} + \begin{bmatrix} C_{55} & 0 \\ 0 & C_{44} \end{bmatrix} \begin{Bmatrix} \frac{\partial w_0}{\partial x} \\ \frac{\partial w_0}{\partial y} \end{Bmatrix} = \begin{Bmatrix} 0 \\ 0 \end{Bmatrix} \tag{16}$$

Eq. (12c):

$$\begin{bmatrix} C_{13} & 0 \end{bmatrix} \begin{Bmatrix} \frac{\partial u_0}{\partial x} \\ \frac{\partial u_0}{\partial y} \end{Bmatrix} + \begin{bmatrix} 0 & C_{23} \end{bmatrix} \begin{Bmatrix} \frac{\partial v_0}{\partial x} \\ \frac{\partial v_0}{\partial y} \end{Bmatrix} + C_{33}\frac{\partial w_0}{\partial z} = \left(C_{13} + C_{23} + C_{33}\right)\alpha\Delta T \tag{17}$$

The physical domain can be transformed into the computational domain using the concept of the domain transformation usually used in the finite element method

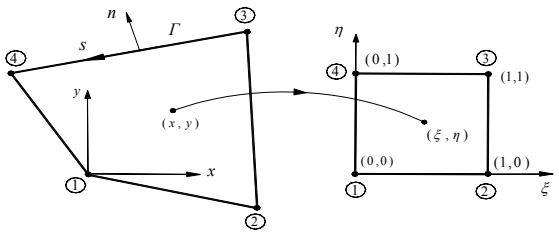

(a) (b)

Fig. 2
Geometry and coordinate system of the FGM plate: a) physical domain, b) computational domain [14-17].

Using the chain rule for the spatial derivatives, one obtains,

$$\begin{Bmatrix} \frac{\partial(\ )}{\partial x} \\ \frac{\partial(\ )}{\partial y} \end{Bmatrix} = \left[T^{11}\right] \begin{Bmatrix} \frac{\partial(\ )}{\partial \xi} \\ \frac{\partial(\ )}{\partial \eta} \end{Bmatrix} \tag{18a}$$

$$\begin{Bmatrix} \frac{\partial^2(\ )}{\partial x^2} \\ \frac{\partial^2(\ )}{\partial y^2} \\ \frac{\partial^2(\ )}{\partial x\,\partial y} \end{Bmatrix} = \left[T^{21}\right] \begin{Bmatrix} \frac{\partial(\ )}{\partial \xi} \\ \frac{\partial(\ )}{\partial \eta} \end{Bmatrix} + \left[T^{22}\right] \begin{Bmatrix} \frac{\partial^2(\ )}{\partial \xi^2} \\ \frac{\partial^2(\ )}{\partial \eta^2} \\ \frac{\partial^2(\ )}{\partial \xi \partial \eta} \end{Bmatrix} \tag{18b}$$

where $\left[T^{11}\right] = \left[J^{11}\right]^{-1}, \left[T^{21}\right] = \left[J^{22}\right]^{-1}\left[J^{21}\right]\left[J^{11}\right]^{-1}, \left[T^{22}\right] = \left[J^{22}\right]^{-1}$ and

$$\left[J^{11}\right] = \begin{bmatrix} \frac{\partial x}{\partial \xi} & \frac{\partial y}{\partial \xi} \\ \frac{\partial x}{\partial \eta} & \frac{\partial y}{\partial \eta} \end{bmatrix} \tag{19a}$$

$$\left[J^{21}\right] = \begin{bmatrix} \frac{\partial^2 x}{\partial \xi^2} & \frac{\partial^2 y}{\partial \xi^2} \\ \frac{\partial^2 x}{\partial \eta^2} & \frac{\partial^2 y}{\partial \eta^2} \\ \frac{\partial^2 x}{\partial \xi \partial \eta} & \frac{\partial^2 y}{\partial \xi \partial \eta} \end{bmatrix} \tag{19b}$$

$$\left[J^{22}\right] = \begin{bmatrix} \left(\frac{\partial x}{\partial \xi}\right)^2 & \left(\frac{\partial y}{\partial \xi}\right)^2 & \frac{\partial x}{\partial \xi}\frac{\partial y}{\partial \xi} \\ \left(\frac{\partial x}{\partial \eta}\right)^2 & \left(\frac{\partial y}{\partial \eta}\right)^2 & \frac{\partial x}{\partial \eta}\frac{\partial y}{\partial \eta} \\ \frac{\partial x}{\partial \xi}\frac{\partial x}{\partial \eta} & \frac{\partial y}{\partial \xi}\frac{\partial y}{\partial \eta} & \frac{1}{2}\left(\frac{\partial x}{\partial \xi}\frac{\partial y}{\partial \eta} + \frac{\partial x}{\partial \eta}\frac{\partial y}{\partial \xi}\right) \end{bmatrix} \tag{19c}$$

Using Eqs. (18a), (18b), the equilibrium equations become, Eq. (7):

$$\begin{aligned} &\left[A^{11}\right] \begin{Bmatrix} \frac{\partial^2 u_0}{\partial \xi^2} \\ \frac{\partial^2 u_0}{\partial \eta^2} \\ \frac{\partial^2 u_0}{\partial \xi \partial \eta} \end{Bmatrix} + \left[A^{12}\right] \begin{Bmatrix} \frac{\partial u_0}{\partial \xi} \\ \frac{\partial u_0}{\partial \eta} \end{Bmatrix} + \left[A^{22}\right] \begin{Bmatrix} \frac{\partial^2 v_0}{\partial \xi^2} \\ \frac{\partial^2 v_0}{\partial \eta^2} \\ \frac{\partial^2 v_0}{\partial \xi \partial \eta} \end{Bmatrix} + \left[A^{21}\right] \begin{Bmatrix} \frac{\partial v_0}{\partial \xi} \\ \frac{\partial v_0}{\partial \eta} \end{Bmatrix} + \begin{Bmatrix} C'_{55}\frac{\partial u_0}{\partial z} + C_{55}\frac{\partial^2 u_0}{\partial z^2} \\ C'_{44}\frac{\partial v_0}{\partial z} + C_{44}\frac{\partial^2 v_0}{\partial z^2} \end{Bmatrix} \\ &+ \left[A^{13}\right] \begin{Bmatrix} \frac{\partial w_0}{\partial \xi} \\ \frac{\partial w_0}{\partial \eta} \end{Bmatrix} + \left[A^{23}\right] \begin{Bmatrix} \frac{\partial^2 w_0}{\partial \xi \partial z} \\ \frac{\partial^2 w_0}{\partial \eta \partial z} \end{Bmatrix} = \begin{Bmatrix} 0 \\ 0 \end{Bmatrix} \end{aligned} \tag{20}$$

Eq. (8):

$$\left[A^{31}\right]\begin{Bmatrix}\dfrac{\partial u_0}{\partial \xi}\\ \dfrac{\partial u_0}{\partial \eta}\end{Bmatrix}+\left[A^{32}\right]\begin{Bmatrix}\dfrac{\partial^2 u_0}{\partial \xi \partial z}\\ \dfrac{\partial^2 u_0}{\partial \eta \partial z}\end{Bmatrix}+\left[A^{33}\right]\begin{Bmatrix}\dfrac{\partial v_0}{\partial \xi}\\ \dfrac{\partial v_0}{\partial \eta}\end{Bmatrix}+\left[A^{34}\right]\begin{Bmatrix}\dfrac{\partial^2 v_0}{\partial \xi \partial z}\\ \dfrac{\partial^2 v_0}{\partial \eta \partial z}\end{Bmatrix}+\left[A^{35}\right]\begin{Bmatrix}\dfrac{\partial^2 w_0}{\partial x^2}\\ \dfrac{\partial^2 w_0}{\partial y^2}\\ \dfrac{\partial^2 w_0}{\partial x\,\partial y}\end{Bmatrix}+\left[A^{36}\right]\begin{Bmatrix}\dfrac{\partial w_0}{\partial \xi}\\ \dfrac{\partial w_0}{\partial \eta}\end{Bmatrix} \tag{21}$$

$$+C_{33}^{'}\frac{\partial w_0}{\partial z}+C_{33}\frac{\partial^2 w_0}{\partial z^2}=\left(C_{33}^{'}\alpha+C_{33}\alpha^{'}\right)\Delta T+C_{33}\alpha\frac{d\left(\Delta T\right)}{dz}$$

Eq. (13):

$$\left[B^{11}\right]\begin{Bmatrix}\dfrac{\partial u_0}{\partial \xi}\\ \dfrac{\partial u_0}{\partial \eta}\end{Bmatrix}+\left[B^{12}\right]\begin{Bmatrix}\dfrac{\partial v_0}{\partial \xi}\\ \dfrac{\partial v_0}{\partial \eta}\end{Bmatrix}+\left(C_{13}n_x^2+C_{23}n_y^2\right)\frac{\partial w_0}{\partial z}=\left[\left(C_{11}+C_{12}+C_{13}\right)n_x^2+\left(C_{12}+C_{22}+C_{23}\right)n_y^2\right]\ \alpha\Delta T \tag{22}$$

Eq. (14):

$$\left[B^{21}\right]\begin{Bmatrix}\dfrac{\partial u_0}{\partial \xi}\\ \dfrac{\partial u_0}{\partial \eta}\end{Bmatrix}+\left[B^{22}\right]\begin{Bmatrix}\dfrac{\partial v_0}{\partial \xi}\\ \dfrac{\partial v_0}{\partial \eta}\end{Bmatrix}+n_x n_y\left(C_{23}-C_{13}\right)\frac{\partial w_0}{\partial z}=n_x n_y\left(C_{11}+C_{13}-C_{22}-C_{23}\right)\alpha\Delta T \tag{23}$$

Eq. (15):

$$\left[B^{31}\right]\begin{Bmatrix}\dfrac{\partial w_0}{\partial \xi}\\ \dfrac{\partial w_0}{\partial \eta}\end{Bmatrix}+C_{55}n_x\frac{\partial u_0}{\partial z}+C_{44}n_y\frac{\partial v_0}{\partial z}=0 \tag{24}$$

Eq. (16):

$$\left[B^{32}\right]\begin{Bmatrix}\dfrac{\partial w_0}{\partial \xi}\\ \dfrac{\partial w_0}{\partial \eta}\end{Bmatrix}+C_{55}\frac{\partial u_0}{\partial z}=0 \tag{25a}$$

$$\left[B^{33}\right]\begin{Bmatrix}\dfrac{\partial w_0}{\partial \xi}\\ \dfrac{\partial w_0}{\partial \eta}\end{Bmatrix}+C_{44}\frac{\partial v_0}{\partial z}=0 \tag{25b}$$

Eq. (17):

$$\left[B^{34}\right]\begin{Bmatrix}\dfrac{\partial u_0}{\partial \xi}\\ \dfrac{\partial u_0}{\partial \eta}\end{Bmatrix}+\left[B^{35}\right]\begin{Bmatrix}\dfrac{\partial v_0}{\partial \xi}\\ \dfrac{\partial v_0}{\partial \eta}\end{Bmatrix}+C_{33}\frac{\partial w_0}{\partial z}=\left(C_{13}+C_{23}+C_{33}\right)\alpha\Delta T \tag{26}$$

Hence, here the differential quadrature method as an efficient and accurate numerical tool is employed to solve these system of equations and consequently, to obtain the initial stress components. A brief review of DQM is presented in Appendix A. The equilibrium Eqs. (20) and (21) can be discretized as [15-17,20-23],

Eq. (20):

$$\begin{aligned}
&\left[A^{11}\right]_k\begin{Bmatrix}\sum_{m=1}^{N_\xi}B^{\xi}_{im}u_{0mjk}\\ \sum_{n=1}^{N_\eta}B^{\eta}_{jn}u_{0ink}\\ \sum_{m=1}^{N_\xi}\sum_{n=1}^{N_\eta}A^{\xi}_{im}A^{\eta}_{jn}u_{0mnk}\end{Bmatrix}+\left[A^{12}\right]_k\begin{Bmatrix}\sum_{m=1}^{N_\xi}A^{\xi}_{im}u_{0mjk}\\ \sum_{n=1}^{N_\eta}A^{\eta}_{jn}u_{0ink}\end{Bmatrix}+\left[A^{22}\right]_k\begin{Bmatrix}\sum_{m=1}^{N_\xi}B^{\xi}_{im}v_{0mjk}\\ \sum_{n=1}^{N_\eta}B^{\eta}_{jn}v_{0ink}\\ \sum_{m=1}^{N_\xi}\sum_{n=1}^{N_\eta}A^{\xi}_{im}A^{\eta}_{jn}v_{0mnk}\end{Bmatrix}\\
&+\left[A^{21}\right]_k\begin{Bmatrix}\sum_{m=1}^{N_\xi}A^{\xi}_{im}v_{0mjk}\\ \sum_{n=1}^{N_\eta}A^{\eta}_{jn}v_{0ink}\end{Bmatrix}+\begin{Bmatrix}\left(C'_{55}\right)_k\sum_{p=1}^{N_z}A^{z}_{kp}u_{0i\,jp}+\left(C_{55}\right)_k\sum_{p=1}^{N_z}B^{z}_{kp}u_{0i\,jp}\\ \left(C'_{44}\right)_k\sum_{p=1}^{N_z}A^{z}_{kp}v_{0i\,jp}+\left(C_{44}\right)_k\sum_{p=1}^{N_z}B^{z}_{kp}v_{0i\,jp}\end{Bmatrix}+\left[A^{13}\right]_k\begin{Bmatrix}\sum_{m=1}^{N_\xi}A^{\xi}_{im}w_{0mjk}\\ \sum_{n=1}^{N_\eta}A^{\eta}_{jn}w_{0ink}\end{Bmatrix}\\
&+\left[A^{23}\right]_k\begin{Bmatrix}\sum_{m=1}^{N_\xi}\sum_{p=1}^{N_z}A^{\xi}_{im}A^{z}_{kp}w_{0mjp}\\ \sum_{n=1}^{N_\eta}\sum_{p=1}^{N_z}A^{\eta}_{jn}A^{z}_{kp}w_{0inp}\end{Bmatrix}=\begin{Bmatrix}0\\0\end{Bmatrix}
\end{aligned} \tag{27}$$

Eq. (21):

$$\begin{aligned}
&\left[A^{31}\right]_k\begin{Bmatrix}\sum_{m=1}^{N_\xi}A^{\xi}_{im}u_{0mjk}\\ \sum_{n=1}^{N_\eta}A^{\eta}_{jn}u_{0ink}\end{Bmatrix}+\left[A^{32}\right]_k\begin{Bmatrix}\sum_{m=1}^{N_\xi}\sum_{p=1}^{N_z}A^{\xi}_{im}A^{z}_{kp}u_{0mjp}\\ \sum_{n=1}^{N_\eta}\sum_{p=1}^{N_z}A^{\eta}_{jn}A^{z}_{kp}u_{0inp}\end{Bmatrix}+\left[A^{33}\right]_k\begin{Bmatrix}\sum_{m=1}^{N_\xi}A^{\xi}_{im}v_{0mjk}\\ \sum_{n=1}^{N_\eta}A^{\eta}_{jn}v_{0ink}\end{Bmatrix}+\\
&\left[A^{34}\right]_k\begin{Bmatrix}\sum_{m=1}^{N_\xi}\sum_{p=1}^{N_z}A^{\xi}_{im}A^{z}_{kp}v_{0mjp}\\ \sum_{n=1}^{N_\eta}\sum_{p=1}^{N_z}A^{\eta}_{jn}A^{z}_{kp}v_{0inp}\end{Bmatrix}+\left[A^{35}\right]_k\begin{Bmatrix}\sum_{m=1}^{N_\xi}B^{\xi}_{im}w_{0mjk}\\ \sum_{n=1}^{N_\eta}B^{\eta}_{jn}w_{0ink}\\ \sum_{m=1}^{N_\xi}\sum_{n=1}^{N_\eta}A^{\xi}_{im}A^{\eta}_{jn}w_{0mnk}\end{Bmatrix}+\left[A^{36}\right]_k\begin{Bmatrix}\sum_{m=1}^{N_\xi}A^{\xi}_{im}w_{0mjk}\\ \sum_{n=1}^{N_\eta}A^{\eta}_{jn}w_{0ink}\end{Bmatrix}+\\
&\left(C'_{33}\right)_k\sum_{p=1}^{N_z}A^{z}_{kp}w_{0i\,jp}+\left(C_{33}\right)_k\sum_{p=1}^{N_z}B^{z}_{kp}w_{0i\,jp}=\left[\left(C'_{33}\alpha+C_{33}\alpha'\right)\Delta T\right]_k+\left[C_{33}\alpha\frac{d\left(\Delta T\right)}{dz}\right]_k
\end{aligned} \tag{28}$$

where A_{ij}^{k} and B_{ij}^{k} $\left(k=\xi,\eta,z\right)$ are the first and the second order DQ weighting coefficients in the *k*-direction, respectively. It should be noted that the matrices $\left[A^{ij}\right]$ are function of the spatial coordinate *z* and they are introduced in Appendix B.

The discretized form of the boundary conditions become [15-17,20-23]

Eq. (22):

$$\left[B^{11}\right]_k\begin{Bmatrix}\sum_{m=1}^{N_\xi}A_{im}^{\xi}u_{0mjk}\\ \sum_{n=1}^{N_\eta}A_{jn}^{\eta}u_{0ink}\end{Bmatrix}+\left[B^{12}\right]_k\begin{Bmatrix}\sum_{m=1}^{N_\xi}A_{im}^{\xi}v_{0mjk}\\ \sum_{n=1}^{N_\eta}A_{jn}^{\eta}v_{0ink}\end{Bmatrix}+\left(C_{13}n_x^2+C_{23}n_y^2\right)\sum_{p=1}^{N_z}A_{kp}^{z}w_{0i\,jp}= \left((C_{11}+C_{12}+C_{13})n_x^2+(C_{12}+C_{22}+C_{23})n_y^2\right)\alpha\Delta T \tag{29}$$

Eq. (23):

$$\left[B^{21}\right]_k\begin{Bmatrix}\sum_{m=1}^{N_\xi}A_{im}^{\xi}u_{0mjk}\\ \sum_{n=1}^{N_\eta}A_{jn}^{\eta}u_{0ink}\end{Bmatrix}+\left[B^{22}\right]_k\begin{Bmatrix}\sum_{m=1}^{N_\xi}A_{im}^{\xi}v_{0mjk}\\ \sum_{n=1}^{N_\eta}A_{jn}^{\eta}v_{0ink}\end{Bmatrix}+n_xn_y\left(C_{23}-C_{13}\right)\sum_{p=1}^{N_z}A_{kp}^{z}w_{0i\,jp}=n_xn_y\left(C_{11}+C_{13}-C_{22}-C_{23}\right)\alpha\Delta T \tag{30}$$

Eq. (24):

$$\left[B^{31}\right]_k\begin{Bmatrix}\sum_{m=1}^{N_\xi}A_{im}^{\xi}w_{0mjk}\\ \sum_{n=1}^{N_\eta}A_{jn}^{\eta}w_{0ink}\end{Bmatrix}+\left(C_{55}n_x\right)\sum_{p=1}^{N_z}A_{kp}^{z}u_{0i\,jp}+\left(C_{44}n_y\right)\sum_{p=1}^{N_z}A_{kp}^{z}v_{0i\,jp}=0 \tag{31}$$

Eq. (25a):

$$\left[B^{32}\right]_k\begin{Bmatrix}\sum_{m=1}^{N_\xi}A_{im}^{\xi}w_{0mjk}\\ \sum_{n=1}^{N_\eta}A_{jn}^{\eta}w_{0ink}\end{Bmatrix}+\left(C_{55}\right)\sum_{p=1}^{N_z}A_{kp}^{z}u_{0i\,jp}=0 \tag{32}$$

Eq. (25b):

$$\left[B^{33}\right]_k\begin{Bmatrix}\sum_{m=1}^{N_\xi}A_{im}^{\xi}w_{0mjk}\\ \sum_{n=1}^{N_\eta}A_{jn}^{\eta}w_{0ink}\end{Bmatrix}+\left(C_{44}\right)\sum_{p=1}^{N_z}A_{kp}^{z}v_{0i\,jp}=0 \tag{33}$$

Eq. (26):

$$\left[B^{34}\right]_k \begin{Bmatrix} \sum_{m=1}^{N_\xi} A_{im}^{\xi} u_{0mjk} \\ \sum_{n=1}^{N_\eta} A_{jn}^{\eta} u_{0ink} \end{Bmatrix} + \left[B^{35}\right]_k \begin{Bmatrix} \sum_{m=1}^{N_\xi} A_{im}^{\xi} v_{0mjk} \\ \sum_{n=1}^{N_\eta} A_{jn}^{\eta} v_{0ink} \end{Bmatrix} + \left(C_{33}\right) \sum_{p=1}^{N_\zeta} A_{kp}^{z} w_{0i\,jp} = \left(C_{13} + C_{23} + C_{33}\right) \alpha \Delta T \tag{34}$$

Other type of boundary conditions can be derived in the same way.

4 NUMERICAL RESULTS

In this part, the numerical results of static analysis of nanocomposite plates under mechanical loading are presented. First of all, to show the accuracy of the above equations and related boundary conditions, our results for maximum deflections are compared with the results of Das et al [18] under uniform pressure in Fig. 3. This figure is presented for $\theta = 75$ and $\frac{a}{b} = 1$. It is obvious that for different loading the results are in an acceptable agreement. It is mentioned that normalized load is defined as follow,

$$P^* = (PL_x^2)/(16Dh) \tag{35}$$

where D is the flexural rigidity, L_x is the length of plate, P is the uniform load and h is the thickness of plate.

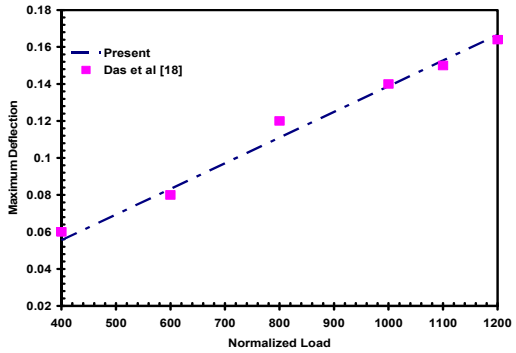

Fig. 3
Comparison of present results with other numerical solution for skew plate.

In Table 1, the maximum deflections of skew nanocomposite plate under uniform pressure is calculated. In this table one can see the influences of two different parameters on the results, 1) Skew angle, 2) Normalized load. It is shown that with the increase of skew angles and with the decrease of uniform load, the maximum vertical deflections will decrease. From this table one can found the importance of skew angle on the calculated results.

The main reason of using three-dimensional elasticity theory is the ability of studying thick nanocomposite plates. So it is important to investigate the effects of thickness on the results. In Table 2, the influences of both thickness and loads are presented for fully clamped skew nanocomposite plate with skew angle of $\theta = 75$. As it is expected, increasing the thickness of nanocomposite plate will decrease the displacements. It can be seen that the thickness of skew nanocomposite plate plays an important role in present analysis.

Table 1
Maximum deflections of skew nanocomposite plate under uniform pressure for different skew angles $(a = b = 1, h = 0.4)$

P^*	$\theta = 50$	$\theta = 60$	$\theta = 70$	$\theta = 80$
800	0.0409	0.0264	0.0136	0.0048
900	0.0461	0.0297	0.0153	0.0054
1000	0.0512	0.033	0.017	0.006
1100	0.0563	0.0363	0.0187	0.0066
1200	0.0614	0.0396	0.0204	0.0072

Table 2
Maximum deflections of skew nanocomposite plate under uniform pressure for different thickness $(a = b = 1)$

P^*	$h = 0.5$	$h = 0.2$	$h = 0.1$	$h = 0.01$
800	0.0075	0.0166	0.0416	11.3371
900	0.0084	0.0187	0.0468	12.7542
1000	0.0093	0.0208	0.0521	14.1713
1100	0.0103	0.0229	0.0573	15.5885
1200	0.0112	0.0250	0.0625	17.0056

Table 3
Stress results of skew nanocomposite plate under uniform pressure for different skew angles $(a = b = 1, h = 0.4)$

P^*	$\theta = 60$	$\theta = 70$	$\theta = 80$
800	127680000	99744000	99692000
900	143640000	112210000	112150000
1000	159600000	124680000	124610000
1100	175560000	137150000	137080000
1200	191520000	149620000	149540000

Table 4
Deflections of nanocomposite plate under uniform pressure for different boundary conditions

a/h	CCCC	CFCF	CSCS
10	10.8445	21.3630	11.2259
11	11.9290	23.4993	12.3485
12	13.0134	25.6356	13.4711
13	14.0979	27.7719	14.5937
14	15.1823	29.9081	15.7163
15	16.2668	32.0444	16.8389
16	17.3512	34.1807	17.9615
17	18.4357	36.3170	19.0841
18	19.5201	38.4533	20.2067
19	20.6046	40.5896	21.3293
20	21.6890	42.7259	22.4519

In Table 3, the effects of skew angles on the σ_z at the center of the skew nanocomposite plate are investigated. One can find from the tabulated results that with the increase of skew angles, the stresses will decrease. From these three tables, one may understand that the major behavior of nanocomposites is the same as ordinary plates. This behavior can be seen in other nano structures such as nanotubes, too. The influences of different boundary conditions on the deflections of nanocomposite plate under uniform pressure are considered in Table 4. Three different boundary conditions are presented, 1) Fully clamped (CCCC), 2) Clamped-Free (CFCF) , 3) Clamped-Simply support (CSCS). In this table, the effects of length to thickness ratio are also investigated. It is shown that the numerical results for fully clamped support are so close to clamped-simply support especially for lower length to thickness ratios. It is also shown that the results of clamped-free support are much more than the results for other boundary conditions. It may be worth to say that the results of clamped-free support are approximately two times bigger than the results for two other boundary conditions. One can also see that increasing the length to thickness ratio will increase the deflections for all boundary conditions. In Fig. 4, we investigate the displacements of nanocomposite plate under sinusoidal mechanical loading. In these figures, one can easily find that increasing the length to thickness ratio will increase the displacements in all directions. It is also shown that increasing the length to width ratio will decrease all the displacements. As it is expected, the displacements in the *Z* direction are much greater than displacements in the *x* and *y* directions.

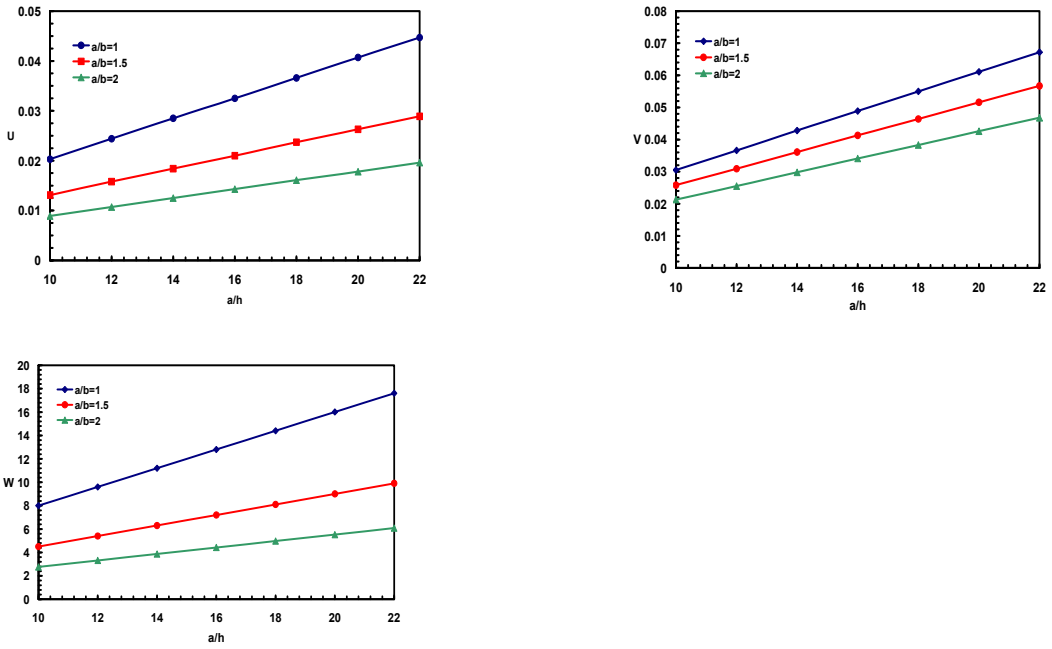

Fig 4.
Deflections of nanocomposite plate subjected to sinusoidal mechanical loading.

5 CONCLUSIONS

In this work, the static behavior of arbitrary straight-sided quadrilateral nanocomposite plates subjected to mechanical loading was presented. Three-dimensional elasticity theory as a suitable theory for investigating both thin and thick plates was used. The differential quadrature method as a numerical tool was adopted to solve the governing equations. Different parameters such as skew angles and thickness of nanocomposite skew plate were studied. As it was expected, it was shown that increasing the skew angle and thickness of nanocomposite skew plate will decrease the vertical displacements. At the end, it is worth to mention that the above equations can be used for all straight-sided quadrilateral nanocomposite plates under both mechanical and thermal loading.

APPENDIX A

DQ weighting coefficients

The DQM [20-23] has attracted appreciable attention over the past two decades. The idea of the DQM is to quickly compute the derivative of a function at any grid point within its bounded domain by estimating a weighted linear sum of values of the function at a small set of points related to the domain. In order to illustrate the DQ approximation, consider a function $f(\xi,\eta)$ having its field on a rectangular domain $0 \le \xi \le a$ and $0 \le \eta \le b$. Let, in the given domain, the function values be known or desired on a grid of sampling points. According to DQ method, the r^{th} derivative of a function $f(\xi,\eta)$ can be approximated as:

$$\left.\frac{\partial^r f(\xi,\eta)}{\partial \xi^r}\right|_{(\xi,\eta)=(\xi_i,\eta_j)} = \sum_{m=1}^{N_\xi} A_{im}^{\xi(r)} f(\xi_m,\eta_j) = \sum_{m=1}^{N_\xi} A_{im}^{\xi(r)} f_{mj} \qquad for\ i=1,2,....N_\xi\ and\ r=1,2,...,N_\xi-1 \tag{A.1}$$

From this equation, one can deduce that the important components of DQ approximations are weighting coefficients and the choice of sampling points. In order to determine the weighting coefficients a set of test functions should be used in Eq. (A.1). For polynomial basis functions DQ, a set of Lagrange polynomials are employed as the test functions. The weighting coefficients for the first-order derivatives in ξ-direction are thus determined as:

$$A_{ij}^{\xi}=\begin{cases}\dfrac{1}{L_{\xi}}\dfrac{M(\xi_i)}{(\xi_i-\xi_j)M(\xi_j)} & \text{for} \quad i\neq j \\ -\sum\limits_{\substack{j=1\\ i\neq j}}^{N_{\xi}} A_{ij}^{\xi} & \text{for} \quad i=j\end{cases} \quad ; \quad i,j=1,2,...,N_{\xi} \tag{A.2}$$

where L_{ξ} is the length of domain along the $\xi-$direction and $M(\xi_i)=\prod\limits_{k=1,i\neq k}^{N_{\xi}}(\xi_i-\xi_k)$

The weighting coefficients of second order derivative can be obtained as,

$$[B_{ij}^{\xi}]=[A_{ij}^{\xi}][A_{ij}^{\xi}]=[A_{ij}^{\xi}]^2 \tag{A.3}$$

In a similar manner, the weighting coefficients for η-direction can be obtained.

In numerical computations, Chebyshev-Gauss-Lobatto quadrature points are used, that is,

$$\frac{\xi_i}{a}=\frac{1}{2}\{1-\cos[\frac{(i-1)\pi}{(N_{\xi}-1)}]\};\quad \frac{\eta_j}{b}=\frac{1}{2}\{1-\cos[\frac{(j-1)\pi}{(N_{\eta}-1)}]\} \qquad for\ i=1,2,\ldots,N_{\xi}\ and\ \ j=1,2,\ldots,N_{\eta} \tag{A.4}$$

APPENDIX B

The matrices $\left[A^{ij}\right]$ *coefficients*

$$A^{11}=\begin{bmatrix}c_{11} & c_{66} & 0\\ 0 & 0 & c_{11}+c_{66}\end{bmatrix}(T^{22}) \tag{B.1}$$

$$A^{12}=\begin{bmatrix}c_{11} & c_{66} & 0\\ 0 & 0 & c_{12}+c_{66}\end{bmatrix}(T^{21}) \tag{B.2}$$

$$A^{22}=\begin{bmatrix}0 & 0 & c_{12}+c_{66}\\ c_{66} & c_{22} & 0\end{bmatrix}(T^{22}) \tag{B.3}$$

$$A^{21}=\begin{bmatrix}0 & 0 & c_{12}+c_{66}\\ c_{66} & c_{22} & 0\end{bmatrix}(T^{21}) \tag{B.4}$$

$$A^{31}=\begin{bmatrix}c_{55} & 0\\ 0 & c_{44}\end{bmatrix}(T^{11}) \tag{B.5}$$

$$A^{23}=\begin{bmatrix}c_{13}+c_{55} & 0\\ 0 & c_{23}+c_{44}\end{bmatrix}(T^{11}) \tag{B.6}$$

$$A^{31}=\begin{bmatrix}c_{13} & 0\end{bmatrix}(T^{11}) \tag{B.7}$$

$$A^{33}=\begin{bmatrix}0 & c_{23}\end{bmatrix}(T^{11}) \tag{B.8}$$

$$A^{32} = \begin{bmatrix} c_{13} + c_{55} & 0 \end{bmatrix} (T^{11}) \tag{B.9}$$

$$A^{34} = \begin{bmatrix} 0 & c_{23} + c_{44} \end{bmatrix} (T^{11}) \tag{B.10}$$

$$A^{35} = \begin{bmatrix} c_{55} & c_{44} & 0 \end{bmatrix} (T^{22}) \tag{B.11}$$

$$A^{36} = \begin{bmatrix} c_{55} & c_{44} & 0 \end{bmatrix} (T^{21}) \tag{B.12}$$

$$B^{11} = \begin{bmatrix} c_{11} n_x^2 + c_{12} n_y^2 & 2c_{66} n_x n_y \end{bmatrix} (T^{11}) \tag{B.13}$$

$$B^{12} = \begin{bmatrix} 2c_{66} n_x n_y & c_{12} n_x^2 + c_{22} n_y^2 \end{bmatrix} (T^{11}) \tag{B.14}$$

$$B^{21} = \begin{bmatrix} (c_{12} - c_{11}) n_x n_y & c_{66} (n_x^2 - n_y^2) \end{bmatrix} (T^{11}) \tag{B.15}$$

$$B^{22} = \begin{bmatrix} c_{66} (n_x^2 - n_y^2) & (c_{22} - c_{12}) n_x n_y \end{bmatrix} (T^{11}) \tag{B.16}$$

$$B^{31} = \begin{bmatrix} c_{55} (n_x) & (c_{44}) n_y \end{bmatrix} (T^{11}) \tag{B.17}$$

$$B^{32} = \begin{bmatrix} c_{55} & 0 \end{bmatrix} (T^{11}) \tag{B.18}$$

$$B^{33} = \begin{bmatrix} 0 & c_{44} \end{bmatrix} (T^{11}) \tag{B.19}$$

$$B^{34} = \begin{bmatrix} c_{13} & 0 \end{bmatrix} (T^{11}) \tag{B.20}$$

$$B^{35} = \begin{bmatrix} 0 & c_{23} \end{bmatrix} (T^{11}) \tag{B.21}$$

REFERENCES

[1] Rieth M., Schommers W., 2005, *Handbook of Theoretical and Computational Nanotechnology,* Basic Concepts, Nanomachines and Bionanodevices, *Forschungszentrum Karlsruhe, Germany* **1**:1-33.

[2] Shariyat M., Darabi E.A., 2013, Variational iteration solution for elastic–plastic impact of polymer/clay nanocomposite plates with or without global lateral deflection, employing an enhanced contact law, *International Journal of Mechanics and Scienc* **67**:14-27.

[3] Jafari Mehrabadi S., Sobhani Aragh B., Khoshkhahesh V., 2012, Mechanical buckling of nanocomposite rectangular plate reinforced by aligned and straight single-walled carbon nanotubes ,*Composite Part B: Engineering* **43**:2031-2040.

[4] Belay O.V., Kiselev S.P., 2011, Molecular dynamics simulation of deformation and fracture of a "copper-molybdenum" nanocomposite plate under uniaxial tension, *Physical Mesomechanics* **14**:145-153.

[5] Yas M.H., Pourasghar A., Kamarian S., 2013, Three-dimensional free vibration analysis of functionally graded nanocomposite cylindrical panels reinforced by carbon nanotube , *Material Design* **49**:583-590.

[6] Moradi-Dastjerdi R., Foroutan M., Pourasghar A., 2013, Dynamic analysis of functionally graded nanocomposite cylinders reinforced by carbon nanotube by a mesh-free method, *Material Design* **44**:256-266.

[7] Heshmati M., Yas M.H., 2013, Dynamic analysis of functionally graded multi-walled carbon nanotube-polystyrene nanocomposite beams subjected to multi-moving loads, *Material Design* **49**:894-904.

[8] Shen H.S., Xiang Y., 2013, Postbuckling of nanotube-reinforced composite cylindrical shells under combined axial and radial mechanical loads in thermal environment *Composite Part B: Engineering* **52**:311-322.

[9] Eftekhari S.A., Jafari A.A., 2013, Modified mixed Ritz-DQ formulation for free vibration of thick rectangular and skew plates with general boundary conditions , *Applied Mathematical Modelling* **37**(12–13):7398–7426.

[10] Upadhyay A.K., Shukla K.K., 2013, Geometrically nonlinear static and dynamic analysis of functionally graded skew plates, *Communications in Nonlinear Science and Numerical Simulation* **18**:2252-2279.

[11] Jaberzadeh E., Azhari M., Boroomand B., 2013, Inelastic buckling of skew and rhombic thin thickness-tapered plates with and without intermediate supports using the element-free Galerkin method, *Applied Mathematical Modelling* **37**(10–11):6838–6854.

[12] Daripa R., Singha M.K., 2009, Influence of corner stresses on the stability characteristics of composite skew plates, *International Journal of Non-Linear Mechanics* **44**(2):138-146.

[13] Kumar N., Sarcar M.S.R., Murthy M.M.M., 2009, Static analysis of thick skew laminated composite plate with elliptical cutout, *Indian Journal of Engineering Material Science* **16**:37-43.

[14] Karami G., Shahpari S.A., Malekzadeh P., 2003, DQM analysis of skewed and trapezoidal laminated plates, *Composite Structure* **59**:393-402.

[15] Malekzadeh P., Karami G., 2006, Differential quadrature nonlinear analysis of skew composite plates based on FSDT, *Engineering Structure* **28**(9):1307-1318.

[16] Malekzadeh P., 2007, A differential quadrature nonlinear free vibration analysis of laminated composite skew thin plates, *Thin-Walled Structure* **45**(2):237-250.

[17] Malekzadeh P., 2008, Differential quadrature large amplitude free vibration analysis of laminated skew plates, on FSDT, *Composite Structure* **83**(2):189-200.

[18] Das D., Sahoo P., Saha K.A., 2009, Variational analysis for large deflection of skew under uniformly distributed load through domain mapping technique, *International Journal of Engineering Science and Technology* **1**:16-32.

[19] Griebal M., Hamaekers J., 2005, Molecular dynamics simulations of the mechanical properties of polyethylene-carbon nanotube composites, *Institut fur Numerische Simulation, Germani.*

[20] Malekzadeh P., 2008, Nonlinear free vibration of tapered Mindlin plates with edges elastically restrained against rotation using DQM, *Thin-Walled Structure* **46**:11-26.

[21] Hashemi M.R., Abedini M.j., Neill S.p., Malekzadeh P., 2008, Tidal and surge modelling using differential quadrature: A case study in the Bristol Channel, *Coastal Engineering* **55**:811-819.

[22] Alibeygi Beni A., Malekzadeh P., 2012, Nonlocal free vibration of orthotropic non-prismatic skew nanoplates, *Composite Structure* **94**:3215-3222.

[23] Malekzadeh P., Heydarpour Y., 2013, Free vibration analysis of rotating functionally graded truncated conical shells, *Composite Structure* **97**:176-188.

[24] Sadd M.H., 2009, *Elasticity, Theory, Applications, and Numerics*, Elsevier.

[25] Griebel M., Hamaekers J., 2004, Molecular dynamics simulations of the elastic moduli of polymer–carbon nanotube composites, *Computer Methods in Applied Mechanics and Engineering* **193**:1773-1788.